

The cosmic ${}^6\text{Li}$ and ${}^7\text{Li}$ problems and BBN with long-lived charged massive particles

Karsten Jedamzik

*Laboratoire de Physique Mathématique et Théorique, C.N.R.S.,
Université de Montpellier II, 34095 Montpellier Cedex 5, France*

Charged massive particles (CHAMPs), when present during the Big Bang nucleosynthesis (BBN) era, may significantly alter the synthesis of light elements when compared to a standard BBN scenario. This is due to the formation of bound states with nuclei. This paper presents a detailed numerical and analytical analysis of such CHAMP BBN. All reactions important for predicting light-element yields are calculated within the Born approximation. Three previously neglected effects are treated in detail: (a) photodestruction of bound states due to electromagnetic cascades induced by the CHAMP decay, (b) late-time efficient destruction/production of ${}^2\text{H}$, ${}^6\text{Li}$, and ${}^7\text{Li}$ due to reactions on charge $Z = 1$ nuclei bound to CHAMPs, and (c) CHAMP exchange between nuclei. Each of these effects may induce orders-of-magnitude changes in the final abundance yields. The study focusses on the impact of CHAMPs on a possible simultaneous solution of the ${}^6\text{Li}$ and ${}^7\text{Li}$ problems. It is shown that a previously suggested simultaneous solution of the ${}^6\text{Li}$ and ${}^7\text{Li}$ problems for a relic decaying at $\tau_x \approx 1000$ sec is only very weakly dependent on the relic being neutral or charged, unless its hadronic branching ratio is $B_h \ll 10^{-4}$ very small. By use of a Monte-Carlo analysis it is shown that within CHAMP BBN the existence of further parameter space for a simultaneous solution of the ${}^6\text{Li}$ and ${}^7\text{Li}$ problem for long decay times $\tau_x \gtrsim 10^6$ sec seems possible but fairly unlikely.

I. INTRODUCTION

Big Bang nucleosynthesis (BBN) is one of the standard pillars of modern cosmology. In its simplest version, reduced to a model with only one parameter, i.e. the contribution of baryons to the critical density, $\Omega_b h^2 \approx 0.0224$ [1], standard BBN predicted and observationally inferred primordial light element abundances are very close. This holds particularly true for ${}^2\text{H}$, and with somewhat less confidence also for ${}^4\text{He}$. However, when the $A > 4$ elements are considered agreement is less convincing. The observationally inferred ${}^7\text{Li}/\text{H}$ ratio is about a factor three smaller than that predicted in SBBN [2]. Moreover, ${}^6\text{Li}$ which is known to only be synthesized at the level ${}^6\text{Li}/\text{H} \sim 10^{-15} - 10^{-14}$ during SBBN has been recently observed in about a dozen metal-poor halo stars with abundance ${}^6\text{Li}/\text{H} \sim 3 - 5 \times 10^{-12}$ [3, 4]. It is tantalizing that these observations indicate a plateau-structure, similar to that observed in ${}^7\text{Li}$, i.e. ${}^6\text{Li}$ abundance independent of metallicity of the star, for stars at the lowest metallicities. A ${}^6\text{Li}$ plateau, should point to a pregalactic or primordial origin of this isotope, since the ${}^6\text{Li}$ had already been in place before stars produced metallicity (and cosmic rays). However, it is cautioned that fairly uncertain stellar pre-main-sequence (PMS) destruction of ${}^6\text{Li}$ could contrive to give an apparent plateau [5].

${}^7\text{Li}$ (as well as ${}^6\text{Li}$) are observed in the atmospheres of metal-poor halo stars. When transported to the hotter interior of the star, by either convection or turbulence, both isotopes may be destroyed. It is thus possible that atmospheric ${}^7\text{Li}$ has been depleted by some factor though standard stellar models do not foresee this. A number of groups have recently re-studied this possibility [6, 7, 8]. Postulating stellar turbulence with a parametrised magnitude, but of unknown origin, Korn *et al* [8] claim that a star-to-star homogeneous factor 1.95 depletion is possible and even favorable when observations of the metal-poor

globular cluster NGC6397 are considered. If true, the remaining factor ~ 1.5 could be either due to systematic errors in the effective stellar temperature calibration or due to an overestimate of the SBBN predicted ${}^7\text{Li}$ abundance due to systematic errors in nuclear reaction data. Concerning the second possibility, a recent remeasurement of the key ${}^7\text{Li}$ producing reaction (${}^3\text{He}(\alpha, \gamma){}^7\text{Be}$) seems to rather indicate a slight underestimate of the synthesized ${}^7\text{Li}$ [9].

${}^6\text{Li}$ is known to be produced by spallation ($p + \text{CNO} \rightarrow \text{LiBeB}$) and fusion ($\alpha + \alpha \rightarrow \text{Li}$) reactions by standard cosmic ray primaries scattering off nucleons and nuclei in the intergalactic medium [10]. Though this process may explain the observed ${}^6\text{Li}$ at solar metallicity, it is clear, however, that it falls short by a large factor (~ 50) to explain the ${}^6\text{Li}$ observed at low metallicity. Similar holds true for putative cosmic ray populations due to shocks developed during structure formation [11]. In order to produce ${}^6\text{Li}/\text{H} \sim 5 \times 10^{-12}$ an early cosmic ray population of $\sim 100\text{eV}/\text{nucleon}$ is required [12]. Most candidate sources fall short of this. The few viable remaining sources are due to accretion on the central Galactic black hole, albeit with an efficiency a factor 10^4 larger than that presently observed, or due to a significant fraction ~ 0.1 of all baryons forming supermassive stars (and cosmic rays) [12]. It may also be that our galaxy was host to a radio-loud quasar some time ago [13]. The energetic problem becomes even exaggerated when likely ${}^6\text{Li}$ destruction during the stellar PMS [5] and putative ${}^6\text{Li}$ destruction during the stellar main-sequence phases are considered, possibly solving the ${}^7\text{Li}$ discrepancy. Finally, it has also been suggested that the ${}^6\text{Li}$ may result in situ from production by solar flares within the first billion of years of the star's life [14]. Though this seems possible, it is hard to evaluate if a sufficient fraction of the freshly synthesized ${}^6\text{Li}$ falls back into the stellar atmosphere rather than being expelled by the solar wind.

It is entirely possible that the ${}^7\text{Li}$ and ${}^6\text{Li}$ anomalies are signs of physics beyond the standard model possibly connected to the quest for the cosmic dark matter. Even very small non-thermal perturbations in the early Universe may lead to a significant and observable ${}^6\text{Li}$ abundance, without overly perturbing other light elements. It had thus been suggested that an anomalous high ${}^6\text{Li}$ abundance is due to non-thermal nuclear reactions (i.e. ${}^3\text{H}(\alpha, n){}^6\text{Li}$, ...) induced by the late-time $t \gtrsim 10^7\text{s}$ electromagnetic [15, 16] or hadronic [17] decay of a relic particle, as for example the gravitino. ${}^6\text{Li}$ in abundance as observed in old stars may also be synthesized due to residual dark matter annihilations during the BBN epoch [18]. In particular, a standard thermal freeze-out process of weak scale particle dark matter (such as supersymmetric neutralinos) is concomitant with the production of ${}^6\text{Li}$ in the right amount, given the dark matter mass falls in the range $20 \lesssim m_\chi \lesssim 90$ GeV, and annihilation is to a significant fraction hadronic and s-wave. Concerning a solution to the ${}^7\text{Li}$ problem, early attempts utilising the electromagnetic decay of a relic and the induced ${}^7\text{Be}$ photodisintegration [19] (${}^7\text{Li}$ is mostly synthesized as ${}^7\text{Be}$, which later on electron-captures) have not proven viable due to unacceptable perturbations in the ${}^2\text{H}/\text{H}$ and ${}^3\text{He}/{}^2\text{H}$ ratios [20]. However, it has been shown that the hadronic decay of a relic during BBN, and the induced excessive neutron abundance may prematurely convert ${}^7\text{Be}$ to ${}^7\text{Li}$ which is then destroyed by proton capture. When $\Omega_\chi B_h \sim 1 - 5 \times 10^{-4}$, where B_h is the hadronic branching ratio, a factor 2 – 4 destruction of ${}^7\text{Li}$ results [21]. For relic decay times $\approx 1000\text{s}$, it is moreover possible to synthesize all the observed ${}^6\text{Li}$ by non-thermal nuclear fusion. This has been the first, and so far only, known simultaneous solution to the ${}^6\text{Li}$ and ${}^7\text{Li}$ problems. It is noted that such a decay also leads to a possibly problematic 30% - 50% increase in the synthesized ${}^2\text{H}/{}^1\text{H}$ ratio.

Within the context of minimal supersymmetric extensions of the standard model of particle physics, a simultaneous solution is nicely realised, either by heavy gravitino decay, or in the case that gravitinos are the lightest supersymmetric particles (LSPs) by the supersymmetric partner of the tau-lepton (the stau) decaying into gravitinos [21]. In the second scenario, an added benefit is that for the right parameters to solve the ${}^6\text{Li}$ and ${}^7\text{Li}$ problems, TeV staus left over from a thermal freeze-out at higher temperature, and decaying at $\tau_x \approx 1000\text{s}$ into 50–100 GeV gravitinos produce naturally about the right amount of gravitinos to explain the dark matter and of a warmness interesting to the formation of large scale structure formation [22]. Unfortunately, staus of mass 1 TeV are too heavy to be discovered at the LHC.

Recently, it has been realised that the existence of electrically charged massive particles (CHAMPs) during the BBN epoch may lead to modifications of the synthesis of light elements [23, 24, 25] beyond those simply due to their decay. Since for gravitino LSPs, the next-to-LSP (NLSP) is long-lived and in about half of the supersym-

metric parameter space it is the electrically charged stau, such effects are important to consider. Other metastable charged relic particles possibly existing during BBN have been also proposed [26]. Modifications to BBN occur due to the formation of electrically bound states between the negatively charged CHAMPs and the positively charged nuclei. The realization that (meta)-stable weak-scale mass charged particles enter into bound states during and after BBN had already been made in the late eighties [27, 28, 29], when the possibility of charged dark matter was analyzed. Nevertheless, the influence of bound states on BBN had not been much discussed.

In this paper results of the up-to-now most detailed calculations of BBN nucleosynthesis in the presence of decaying negatively charged particles are presented. The analysis attempts to reveal all key processes important for a reliable prediction of light element yields, thereby revealing, heretofore neglected effects, which make orders of magnitude changes in the predicted BBN yields for much of the parameter space. These changes are found mostly for late decaying $\tau_x \gtrsim 10^6\text{s}$ CHAMPs. The aim of the paper is to analyze the potential of bound-state nucleosynthesis to solve the cosmic ${}^7\text{Li}$ and ${}^6\text{Li}$ problems.

The outline of the paper is as follows. In Section 2 a discussion/analysis of all priorly suggested solutions to the ${}^7\text{Li}$ problem within bound-state nucleosynthesis is presented, whereas in Section 3 details of the present calculations are given. In Section 4 it is shown that BBN continues to very low temperatures $T \ll 1\text{keV}$ in the presence of bound states. Section 5 shows that bound states are efficiently photodisintegrated already at high temperature due to the decay of the relic. Section 6 stresses the importance of CHAMP transfer reactions at late times. Finally In Section 7 possible further solutions to the ${}^6\text{Li}$ and ${}^7\text{Li}$ problems for late-decaying CHAMPs $\tau_x \gtrsim 10^6\text{sec}$ are discussed. Section 8 draws the conclusions. An appendix gives some detail on the determination of reaction rates in the Born approximation.

II. BOUND-STATE BBN AND PRIOR SUGGESTED SOLUTIONS TO THE ${}^7\text{Li}$ PROBLEM

Modifications to BBN occur due to the formation of electrically bound states between the negatively charged CHAMPs and the positively charged nuclei. Since bound state binding energies may be appreciable (cf. Table 1), a significant fraction of ${}^7\text{Be}$ may be captured by CHAMPs at temperatures as high as $T \lesssim 30\text{keV}$, whereas the same occurs at $T \lesssim 10\text{keV}$ for ${}^4\text{He}$. This may be seen in Fig. 1, which shows the fractions $f_i^b = n_{(N_i X^-)}/n_{N_i}^{\text{tot}}$ of ${}^7\text{Be}$, ${}^7\text{Li}$, ${}^6\text{Li}$, and ${}^4\text{He}$ locked up within bound states. On first sight, the most important effect of bound states during BBN is a reduction of the Coulomb barrier [23, 24]. Nevertheless, since SBBN is essentially finished at $T \approx 10\text{keV}$, Coulomb barrier modifications of reactions rates involving ${}^4\text{He}$ should be hardly important (even though,

ad hoc, speculated otherwise in Ref. [24]). However, as shown by Pospelov [23] there is a non-trivial catalytic effect on reactions involving photons in the final state. SBBN reaction rates involving dipole radiation (E1; e.g. ${}^3\text{He}({}^4\text{He}, \gamma){}^7\text{Be}$) scale as λ_γ^{-3} , whereas reaction rates forbidden at the dipole approximation but allowed at quadrupole (E2; e.g. ${}^2\text{H}({}^4\text{He}, \gamma){}^6\text{Li}$) scale as λ_γ^{-5} , where λ_γ is the wavelength of the emitted photon. This, in both cases is around $\sim 130\text{ fm}$. In the presence of a ${}^4\text{He}$ -CHAMP bound state the reaction may proceed photonless (e.g., ${}^2\text{H}({}^4\text{He}-X^-, X^-){}^6\text{Li}$) and λ_γ is approximately replaced by the Bohr radius $a_{4\text{He}}$ of the ${}^4\text{He}$ -CHAMP bound system. Since $a_{4\text{He}} \approx 4.8\text{ fm}$ (cf. Table 1) very large enhancement factors of 7×10^7 and 3×10^5 [23, 30] for the S-factors of the ${}^2\text{H} + {}^4\text{He}$, and ${}^3\text{He} + {}^4\text{He}$ reactions, respectively, have been estimated. A recent more detailed three-body nuclear reaction calculation of the ${}^2\text{H} + {}^4\text{He}$ reaction, has reduced this estimate by a factor ~ 10 [31]. Such large enhancement factors are important as they lead to excessive ${}^6\text{Li}$ (and ${}^7\text{Li}$) production for any weak scale charged particles which are sufficiently long-lived $\tau_x \gtrsim 4 \times 10^3\text{ s}$, unless $\Omega_X \lesssim 3 \times 10^{-6}$. They have thus been utilised to place a stringent upper limit on the reheat temperature in the early Universe $T \lesssim 10^7\text{ GeV}$ in the case when the supersymmetric gravitino exists and when it is the LSP [32]. Nevertheless, it seems somewhat premature to set such upper limits, as the BBN with charged long-lived particles for decay times $\tau_X \gtrsim 10^6\text{ s}$ had priorly not been investigated (cf. Section 8).

The putative existence of bound states during BBN has also led to a flood of claims of possible solutions to the ${}^7\text{Li}$ and/or ${}^6\text{Li}$ anomalies. In Ref. [24] it was realized that significant fractions of the ${}^7\text{Be}$ and ${}^7\text{Li}$ isotopes are within bound states during BBN. This has lead the authors to arbitrarily enhance certain reactions rates involving mass-7 element destruction processes by large factors, leading to the claim that the existence of bound states may solve the ${}^7\text{Li}$ overproduction problem. However, these claims are, up to now, unfounded [33] (see also below). In Ref. [25] it was noted that during the decay of X^- , when residing in a bound state with ${}^4\text{He}$, the ${}^4\text{He}$ nucleus could break up. The resultant energetic ${}^3\text{H}$ and ${}^3\text{He}$ could then fuse on ${}^4\text{He}$ to produce ${}^6\text{Li}$, in a similar to what had been proposed in [15, 17]. Though the suggestion is correct, the authors calculate the break-up probability to be very small (cf. also Ref. [35]), such that the ${}^6\text{Li}$ synthesis by catalytic ${}^2\text{H}({}^4\text{He}-X^-, X^-){}^6\text{Li}$ is by far dominant. The analysis of Ref. [30] (and Ref. [34]) essentially confirms the simultaneous solutions to the ${}^6\text{Li}$ and ${}^7\text{Li}$ problems as given in Ref. [21, 22], even when bound state effects are included. In Ref. [36] the case of almost degenerate NLSP staus $\tilde{\tau}$ and LSP neutralinos $\tilde{\chi}$ has been considered. Here mass splittings smaller than $\delta m = m_{\tilde{\tau}} - m_{\tilde{\chi}} \lesssim 1\text{ GeV}$ have been assumed. In this region of $\tilde{\tau}$ - $\tilde{\chi}$ parameter space, motivated by the well-known $\tilde{\tau}$ - $\tilde{\chi}$ coannihilation region for neutralino dark matter, the stau is relatively long-lived due to final phase

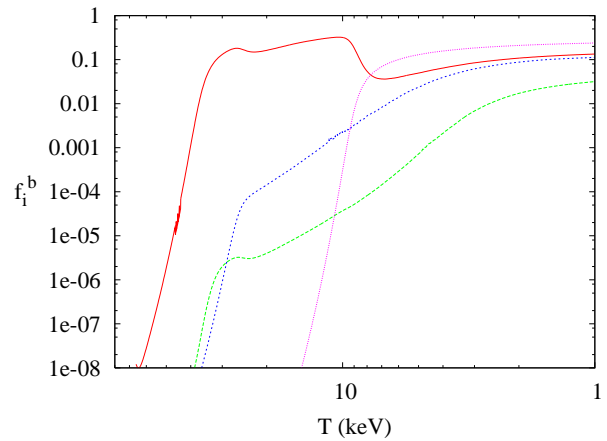


FIG. 1: Bound state fractions $f_i^b \equiv n_{(N_i X^-)}/n_{N_i}^{tot}$ of nuclei N_i bound to CHAMP X^- as a function of temperature T , for a model with $M_X = 100\text{ GeV}$ and $\Omega_X h^2 = 0.1$ (corresponding to a CHAMP-to-baryon ratio $Y_{X^-} = 4.26 \times 10^{-2}/2$). Shown are f_i^b for ${}^7\text{Be}$ solid (red), ${}^7\text{Li}$ long-dashed (green), ${}^6\text{Li}$ short-dashed (blue), and ${}^4\text{He}$ dotted (purple), respectively. Nuclear destruction of bound states results in a behaviour of f_i^b different than that expected from simple estimates by the Saha equation. This is particularly seen in f_i^b for ${}^7\text{Li}$ due to the ${}^1\text{H}({}^7\text{Li}-X^-, X^-){}^4\text{He} + {}^4\text{He}$ reaction.

space suppression of the decay. It is claimed, that the ${}^7\text{Li}$ overproduction problem may be solved by internal conversion of staus in bound states with ${}^7\text{Be}$, to neutralinos, e.g. $(\tilde{\tau}-{}^7\text{Be}) \rightarrow \tilde{\chi} + \nu_\tau + {}^7\text{Li}$ and the subsequent destruction of ${}^7\text{Li}$ by protons. It is argued that solutions to the ${}^7\text{Li}$ problem may be found for $\delta m \lesssim 100\text{ MeV}$ even for the smallest abundances of staus. A more detailed analysis of the ${}^7\text{Be}$ -bound state fraction via the Boltzmann equation shows, however, that only a very small fraction of ${}^7\text{Be}$ are within bound states, thus making modifications of the ${}^7\text{Li}$ abundance at low stau-density negligible. At larger stau-densities some effect may result.

Ref. [35] make the interesting suggestion that the ${}^7\text{Li}$ problem could be solved by catalytic conversion of ${}^7\text{Be}$ via $({}^7\text{Be}-X^-)(p, \gamma)({}^8\text{B}-X^-)$ and the subsequent beta-decay of the ${}^8\text{B} \rightarrow {}^8\text{Be} + e^+ + \nu_e$ nucleus. This reaction would mostly occur via a p - ${}^7\text{Be}$ resonance in the ${}^8\text{B}$ nucleus which, in the absence of bound states lies at 769.5 keV relative to the p - ${}^7\text{Be}$ continuum. The catalysm in the reaction would then occur by a shifting of the resonance to $\approx 167\text{ keV}$ relative to the p -(${}^7\text{Be}-X^-$) continuum since the $({}^8\text{B}-X^-)$ bound state binding energy ($E_{s_{\text{B}X^-}} \approx 2.0\text{ MeV}$) is larger than that of ${}^7\text{Be}$ ($E_{\tau_{\text{Be}X^-}} \approx 1.39\text{ MeV}$), making the resonance available at only slightly supra-thermal energies. Moreover, apart from the decrease in the resonance energy they also deduce a factor $\sim 10^3$ larger reaction rate coefficient. Adopting their calculated rates for ${}^7\text{Be}-X^-$ bound state formation and the $({}^7\text{Be}-X^-)(p, \gamma)({}^8\text{B}-X^-)$ reaction, I partially confirm this effect by full numerical analysis. For example, for $\tau_X = 1.5 \times 10^3\text{ s}$ and the number ratio

of X^- s to baryons $Y_X \approx 0.2$, I find a reduction of the ${}^7\text{Li}$ abundance by 33%, and a ${}^6\text{Li}/\text{H}$ ratio of 2×10^{-11} . However, the effect is not as strong as initially imagined, since by the reciprocity theorem the inverse rate is also enhanced. The inverse rate $1/\tau_{\text{inv}}$ is thus around 10^3 times larger at $T \approx 32.5\text{ keV}$ than the beta decay rate $1/\tau_\beta$ of ${}^8\text{B}$ (half-time of 770 ms), converting ${}^8\text{B}-X^-$ rapidly back to ${}^7\text{Be}-X^- + p$, before ${}^8\text{B}$ can beta-decay. The effect is therefore essentially absent at early times (i.e. small τ_X). Nevertheless, the inverse rate quickly drops below the beta decay rate (i.e. $\tau_\beta/\tau_{\text{inv}} \approx 0.1$ at $T \approx 24.1\text{ keV}$). For the same parameters as above, I still find a 14% reduction of the final ${}^7\text{Li}$. This drops to 7%, 2% for $\tau_X = 10^3$ and $7 \times 10^2\text{ s}$, respectively.

It is interesting to know if the solution of the lithium problems proposed in Ref. [21] is changed when the decaying relic is charged, such as the stau. In Fig. 2 the parameter space solving either the ${}^7\text{Li}$ problem, or both the ${}^6\text{Li}$ and ${}^7\text{Li}$ problems, is shown. The upper panel shows results for a charged relic and the lower panel for a neutral relic. Here observational limits as discussed in Ref. [37] have been applied and the ${}^6\text{Li}$, ${}^7\text{Li}$ problems are assumed to be reconciled with observational data for ${}^6\text{Li}/{}^7\text{Li} \gtrsim 0.03$ and ${}^7\text{Li}/\text{H} \lesssim 2.5 \times 10^{-10}$. The assumed parameters of the model are a hadronic branching ratio $B_h = 10^{-4}$ and relic mass $M_X = 1\text{ TeV}$. It is seen that even at B_h as small as 10^{-4} the ${}^7\text{Li}$ -solving region is essentially unmodified, whereas some changes are observed in the ${}^6\text{Li}$ and ${}^7\text{Li}$ solving regions. These latter are mostly due to excessive ${}^6\text{Li}$ production when the relic is charged, disallowing some of the larger life times $\tau_X \gtrsim 2 \times 10^4\text{ s}$. Bound state effects are nevertheless important when the hadronic branching ratio is very small. This may be seen in the lowest panel of Fig. 2, where $B_h = 0$ has been assumed. When only bound state effects are operative, the ${}^2\text{H}/{}^1\text{H}$ -ratio is essentially unmodified. This is in contrast to the solution of the lithium problems with a hadronic decay, as seen by the dotted (blue) lines in the upper two panels, beyond which ${}^2\text{H}/{}^1\text{H}$ is larger than 4×10^{-5} . It is intriguing that both processes, hadronic decay and bound state effects, have the same preferred τ_X for a simultaneous solution of the lithium problems.

III. DETAILED BOUND-STATE BBN CALCULATIONS

The calculations presented here attempt to take proper account of the influence of singly bound states on the nucleosynthesis for elements with nucleon number $A \leq 7$. Heavier elements as well as the formation of molecules, such as $(X^- - {}^4\text{He} - X^-)$, are not considered. All effects of electromagnetic and hadronic cascade nucleosynthesis are included and treated as presented in Ref. [37]. The fractions of individual nuclei i in bound states $f_i^b = n_{(N_i X^-)}/n_{N_i}^{\text{tot}}$ are computed by full numerical integration of the Boltzman equation. This is required since estimates by the Saha equation are only very approximative,

TABLE I: Nucleus, energy of bound state, approximative Bohr radius of bound state a_B [38], and adopted root-mean-square charge radius for nucleus

nucleus	E_b (keV)	$\approx a_B$ (fm)	$\langle r^2 \rangle_c^{1/2}(\text{fm})$
${}^1\text{H}$	24.97	28.8	0.895
${}^2\text{H}$	49.5	14.4	1.3
${}^3\text{H}$	72.6	9.6	1.7
${}^3\text{He}$	269	5.2	1.951
${}^4\text{He}$	349.6	4.8	1.673
${}^6\text{Li}$	842.5	2.1	2.37
${}^7\text{Li}$	897.6	1.9	2.50
${}^7\text{Be}$	1385	1.5	2.50

due to the relatively early freeze-out of the CHAMP-nuclei recombination process [24]. Except of the recombination rate of X^- on ${}^7\text{Be}$, which is taken from Ref. [35], all other recombination rates are computed by a numerical integration of the Schroedinger equation. This may make difference up to a factor two in f_i^b since the recombination rates as given in Ref. [24] only apply asymptotically at low temperature T . Bound state wave functions and bound-state energies are also computed by an integration of the Schroedinger equation, assuming realistic charge radii for the nucleus as measured by experiment. The reader is referred to Table 1, for some of the bound state properties. Finally, it is important, to take into account the nuclear destruction of bound states. Nuclear rates are very fast at early times, and for reaction which are sufficiently exothermic, the electric bound between the final nucleus (nuclei) ought to be destroyed [39]. This often changes f_i^b by orders of magnitude.

A proper evaluation of BBN yields with bound states is only possible when somewhat realistic nuclear reaction rates for nuclei within bound states are present. With the exception of the reaction ${}^2\text{H}({}^4\text{He}-X^-, X^-){}^6\text{Li}$ a more detailed evaluation of such reactions had been absent of the literature so far. Improving over simple scaling relations [23, 30] seems important also, since nuclear reactions including bound states contain three quantities of similar magnitude, a_B the Bohr radius, a_{nucl} the nuclear radius, and k_f the momentum of the outgoing nucleus. All three quantities are in the several Fermi range, thus leading potentially to important cancellation effects. More importantly, estimates via simple scaling relations adopt the Born approximation, which is known to fail at low energies and strong perturbations [40]. This is essentially the case for all reactions of importance to bound-state BBN. The failure of the Born approximation had been seen, for example, by the reduction of the ${}^2\text{H}({}^4\text{He}-X^-, X^-){}^6\text{Li}$ rate by a factor ~ 10 , when a more detailed evaluation [31] is compared to a simple scaling result.

I have identified all key reactions in bound-state BBN.

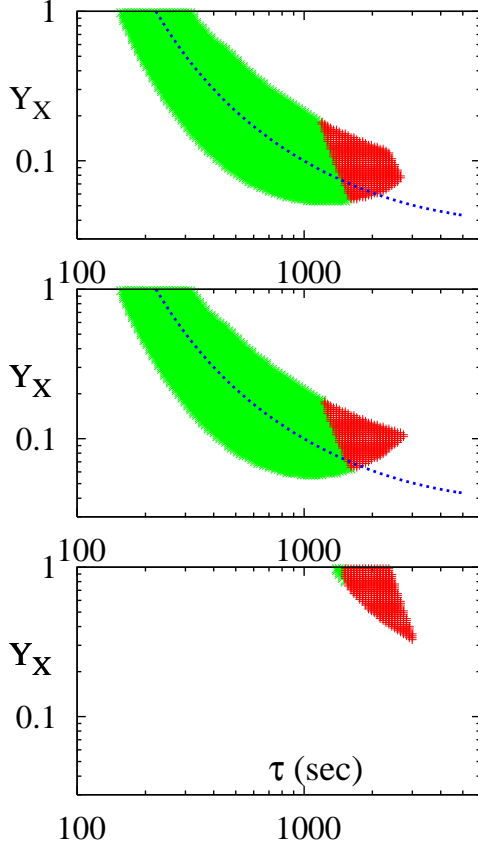


FIG. 2: Parameter space in the relic particle-to-baryon ratio Y_X and relic particle decay time τ_X which may resolve either the ${}^7\text{Li}$ problem (green - light) or both, the ${}^7\text{Li}$ and ${}^6\text{Li}$ problems (red - dark). The panels show, from top to bottom: (a) a charged relic with $B_h = 10^{-4}$, (b) a neutral relic with $B_h = 10^{-4}$, and (c) a charged relic with $B_h = 0$. All three panels assume a mass $M_x = 1\text{ TeV}$ for the relic. By comparison of the green (lighter) areas it is seen that bound-state effects on ${}^7\text{Li}$, as suggested in Ref. [35], do not have a very big impact for relic hadronic branching ratios $B_h \gtrsim 10^{-4}$. The adopted abundance limits are: ${}^2\text{H}/{}^1\text{H} < 5.3 \times 10^{-5}$, ${}^7\text{Li}/{}^1\text{H} < 2.5 \times 10^{-10}$, ${}^6\text{Li}/{}^7\text{Li} < 0.66$, and ${}^6\text{Li}/{}^7\text{Li} > 0.03$ to solve the ${}^6\text{Li}$ problem. Above the dotted lines the ${}^2\text{H}/{}^1\text{H}$ ratio exceeds a value of 4×10^{-5} .

These are shown in Table 2. It is completely beyond the scope of the present paper to evaluate all these reaction rates more properly, i.e. beyond the Born approximation, a task which is formidable in particular when the important CHAMP-exchange reactions (cf. Section 6) are also considered. For the ${}^2\text{H}({}^4\text{He}-X^-, X^-){}^6\text{Li}$ process the rate as given by Ref. [31] was adopted. For other reactions, as a starting point, I have thus nevertheless, evaluated rates in the Born approximation. These rates will serve as benchmarks later on. For details concerning these calculations the reader is referred to Appendix A. Results for the in such a way obtained S-factors are

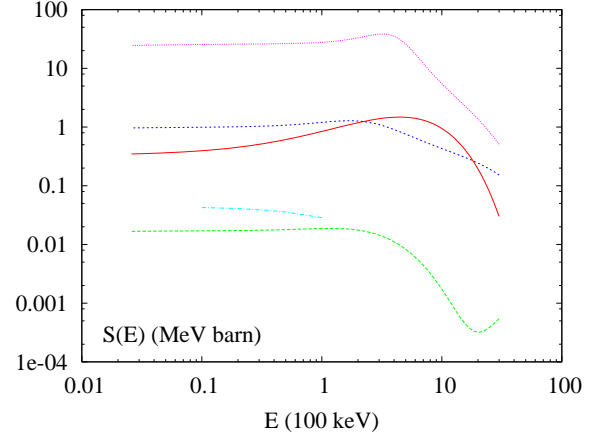


FIG. 3: Nuclear reaction $S(E)$ -factors as function of energy computed in the present analysis. The most important S -factors for nuclear reactions involving the $({}^4\text{He}-X^-)$ bound state are shown: ${}^2\text{H}({}^4\text{He}-X^-, X^-){}^6\text{Li}$ solid (red), ${}^3\text{H}({}^4\text{He}-X^-, X^-){}^7\text{Li}$ short-dashed (blue), and ${}^3\text{He}({}^4\text{He}-X^-, X^-){}^7\text{Be}$ dotted (purple), respectively. The dashed-dotted (light-blue) line shows the result of a recent evaluation [31] of ${}^2\text{H}({}^4\text{He}-X^-, X^-){}^6\text{Li}$, whereas the long-dashed (green) line shows the result for the same reaction computed in this paper when the $l = 1$ and $l = 2$ contributions are neglected.

TABLE II: Assumed properties for the calculation of nuclear reactions with one nuclei in a bound state. The columns show: Reaction, S -factor for the SBBN reaction in MeV barn, angular momentum for the $(AB) = C$ final bound nucleus, and the multipoles for the initial Coulomb wave which are included in the calculation.

No.	$(AX) + B \rightarrow C + X$	S_γ	l_C	l_{Coul}^i
1	$({}^4\text{He}-X^-) + {}^2\text{H} \rightarrow {}^6\text{Li} + X^-$	10^{-8}	0	0,1,2
2	$({}^4\text{He}-X^-) + {}^3\text{H} \rightarrow {}^7\text{Li} + X^-$	8×10^{-5}	1	0,1
3	$({}^4\text{He}-X^-) + {}^3\text{He} \rightarrow {}^7\text{Be} + X^-$	4×10^{-4}	1	0,1
4	$({}^1\text{H}-X^-) + {}^6\text{Li} \rightarrow {}^7\text{Be} + X^-$	10^{-4}	1	0,1
5	$({}^1\text{H}-X^-) + {}^6\text{Li} \rightarrow {}^4\text{He} + {}^3\text{He} + X^-$	3	-	-
6	$({}^1\text{H}-X^-) + {}^7\text{Li} \rightarrow ({}^8\text{Be}-X^-) + \gamma$	10^{-3}	1	0,1
7	$({}^1\text{H}-X^-) + {}^7\text{Be} \rightarrow {}^8\text{B} + X^-$	3×10^{-5}	1	0,1
8	$({}^2\text{H}-X^-) + {}^4\text{He} \rightarrow {}^6\text{Li} + X^-$	10^{-8}	0	0,1,2
9	$({}^3\text{H}-X^-) + {}^4\text{He} \rightarrow {}^7\text{Li} + X^-$	8×10^{-5}	1	0,1

shown in Fig. 3 and Fig. 4, respectively.

IV. LATE-TIME BOUND-STATE BIG BANG NUCLEOSYNTHESIS

The reader may have noted that Table 2 also includes reactions with bound states on elements ${}^1\text{H}, {}^2\text{H}, {}^3\text{H}$ with only one charge number $Z = 1$. In fact, such reactions are extremely important at low temperatures $T \lesssim 3, 2, 1\text{ keV}$

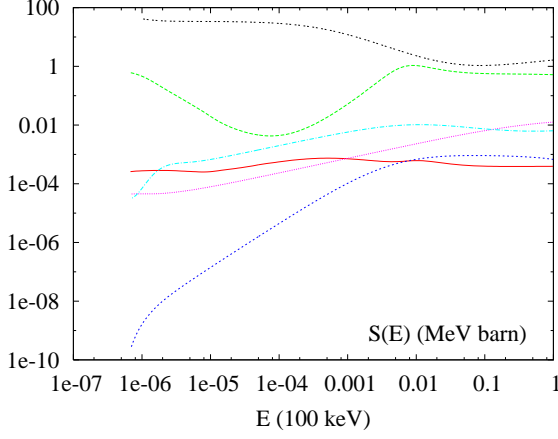


FIG. 4: Nuclear reaction $S(E)$ -factors as function of energy computed in the present analysis. The most important S -factors for nuclear reactions involving bound states with $Z = 1$ nuclei are shown: (from top to bottom at the highest energies) ${}^6\text{Li}({}^1\text{H}-X^-, X^-){}^4\text{He}+{}^3\text{He}$ double-dotted (black), ${}^7\text{Be}({}^1\text{H}-X^-, X^-){}^8\text{B}$ long-dashed (green), ${}^4\text{He}({}^3\text{H}-X^-, X^-){}^7\text{Li}$ dotted (purple), ${}^4\text{He}({}^2\text{H}-X^-, X^-){}^6\text{Li}$ dash-dotted (light-blue), ${}^7\text{Li}({}^1\text{H}-X^-, \gamma){}^8\text{Be} - X^-$ short-dashed (blue), and ${}^6\text{Li}({}^1\text{H}-X^-, X^-){}^7\text{Be}$ solid (red).

when one after the other, non-negligible fraction of ${}^3\text{H}$, ${}^2\text{H}$, and ${}^1\text{H}$ enter into bound states. This may be seen in Fig. 5. It is noted here, that a possible impact of such reactions has been pointed out before [24], albeit in a very approximative way. It was not clear, a priori, if the Coulomb barrier between, for example, ${}^1\text{H}$ and ${}^6\text{Li}$ is sufficiently suppressed in order to make reactions such as ${}^6\text{Li}({}^1\text{H}-X^-, X^-){}^4\text{He} + {}^3\text{He}$ efficient enough to substantially reduce any priorly synthesized ${}^6\text{Li}$. This is because, on first sight, Coulomb shielding of the proton could only be partial, due to the fairly extended Bohr radius $a_B \approx 29$ fm of the ${}^1\text{H}-X^-$ system. In Fig. 6 a $l = 0$ spherical wave without any Coulomb repulsion, i.e. $V_c = 0$, is compared to the spherical Coulomb wave functions between the ${}^6\text{Li}$ and the ${}^1\text{H}-X^-$ bound state with $l = 0$ and $l = 1$ initial angular momentum, respectively. It is seen that essentially no Coulomb suppression exists. Rather, the incoming wave function of the ${}^6\text{Li}$ nuclei is even strongly enhanced at the center. This is not surprising, as by assumption, the X^- resides at the center, and due to the significant spread in the wave function of the proton ($a_B \approx 29$ fm) the effective proton charge density at the center is low. The Coulomb potential for the ${}^6\text{Li}$ nucleus is $\phi_{\text{Li}} = -3e^2 \exp(-2r/a_B)(1/r + 1/a_B)$, thus very attractive at the center and approaching zero at large distances. Nuclear reactions between such bound states and bare nuclei, are therefore not Coulomb suppressed. It is rather conceivable, that Coulomb focussing occurs at low energies, even enhancing the reaction rates over the $V_C = 0$ case. This may be observed in the S -factor for the $({}^1\text{H}-X^-) + {}^6\text{Li} \rightarrow {}^4\text{He} + {}^3\text{He} + X^-$ reaction as shown in Fig. 4. It is noted here, that due to an anomalously

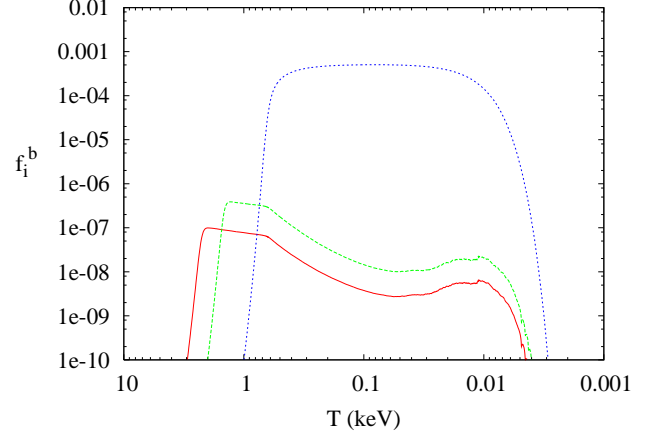


FIG. 5: Bound state fractions f_i^b for ${}^3\text{H}$ (solid - red), ${}^2\text{H}$ (dashed - green), and ${}^1\text{H}$ (blue - dotted) as a function of temperature T . Adopted model parameters are as in Fig. 1 with a X decay time $\tau_X = 10^{10}$ s. For illustrative purposes photo-disintegration of bound states due to X -decay (cf. Section 5) and X -exchange reactions (cf. Section 6) have not been taken into account.

low ${}^7\text{Li}({}^1\text{H}-X^-, X^-){}^8\text{Be}$ rate found in the Born approximation the rate for ${}^7\text{Li}({}^1\text{H}-X^-, \gamma){}^8\text{Be}-X^-$ has been computed and utilised in the calculations.

Thus, $Z = 1$ bound states at $T \approx 1$ keV behave almost as neutrons (with the exception that they are stable). Already very small fractions of these bound states induce therefore a second round of late-time nucleosynthesis, capable of destroying all the synthesized ${}^6\text{Li}$, ${}^9\text{Be}$, and some of the ${}^7\text{Li}$. This may be seen in Fig. 7 where the ${}^6\text{Li}/\text{H}$, ${}^7\text{Li}/\text{H}$, ${}^7\text{Be}/\text{H}$, and ${}^2\text{H}/\text{H}$ ratios are shown for a CHAMP with $\Omega_X h^2 = 0.01$, $m_X = 100$ GeV, and decay time $\tau_X = 10^{10}$ s, where h is the dimensionless present-day Hubble parameter, and Ω_X [41] the fractional contribution of CHAMPs to the present critical density, would they not have decayed. Note, that this is easily converted to the CHAMP-to-baryon ratio $Y_X = (\Omega_X h^2 / \Omega_b h^2)(m_p / m_X)$ which is $Y_X \approx 4.26 \times 10^{-3}$ for the adopted parameters. The calculations presented in Fig. 7 (as well as Figs. 1 and 5) are performed under the assumption that the X decay is not associated with any electromagnetic- or hadronic- energy release and in the absence of X -exchange reactions (cf. Section 6). This is done to isolate the effects of the bound states. At early times, towards the end of conventional BBN, when a significant fraction of ${}^4\text{He}$ enters bound states, the reactions ${}^2\text{H}({}^4\text{He}-X^-, X^-){}^6\text{Li}$, ${}^3\text{H}({}^4\text{He}-X^-, X^-){}^7\text{Li}$, and ${}^3\text{He}({}^4\text{He}-X^-, X^-){}^7\text{Be}$, synthesize significant, and observationally completely unacceptable abundances of the $A > 4$ isotopes. However, when bound states of the $Z = 1$ elements form at $T \approx 1$ keV, essentially all the synthesized ${}^6\text{Li}$ and ${}^7\text{Be}$ may be rapidly destroyed by the reactions ${}^6\text{Li}({}^1\text{H}-X^-, X^-){}^4\text{He} + {}^3\text{He}$ and ${}^7\text{Be}({}^1\text{H}-X^-, X^-){}^8\text{B}$. The situation appears different for ${}^7\text{Li}$, due to the small estimate for

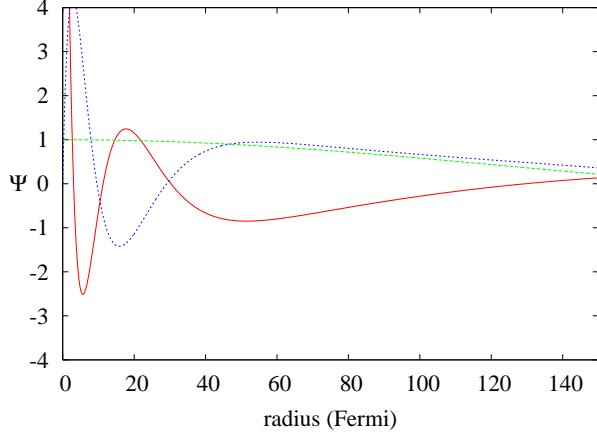


FIG. 6: Spherical Coulomb wave functions of a ${}^6\text{Li}$ nuclei with energy $E = 1\text{ keV}$ in the electric field of the ${}^1\text{H}-X^-$ bound state, for s-wave (angular momentum $l = 0$ - solid - red) and p-wave (angular momentum $l = 1$ - dotted - blue) where X^- is at radius $r = 0$. For comparison the spherical wave function without any Coulomb barrier, i.e. $V_C = 0$, for s-wave, is also shown (dashed - green). It is seen that no significant Coulomb barrier suppression of the wave function near the origin exists. Rather, both Coulomb wave functions are significantly enhanced at the center, due to the presence of X^- at $r = 0$. The oscillatory behaviour may lead to important interference effects. Both, the $l = 0$ and $l = 1$ initial states have significant contributions to the cross section.

the ${}^7\text{Li}({}^1\text{H}-X^-, X^-){}^8\text{Be}$ and ${}^7\text{Li}({}^1\text{H}-X^-, \gamma){}^8\text{Be}-X^-$ cross sections, implying that almost all initially synthesized ${}^7\text{Li}$ is left intact [42]. The abundance of ${}^7\text{Li}/\text{H}$ is found at an observationally friendly 2.7×10^{-10} . It is noted that ${}^2\text{H}$ is also destroyed, though to a much smaller degree, mostly by the reactions ${}^3\text{H}({}^2\text{H}-X^-, n){}^4\text{He}+X^-$, ${}^3\text{He}({}^2\text{H}-X^-, p){}^4\text{He}+X^-$, and ${}^2\text{H}({}^3\text{H}-X^-, n){}^4\text{He}+X^-$, and to a lesser degree by ${}^2\text{H}({}^1\text{H}-X^-, X^-){}^3\text{He}$. The reader is referred to Table 3 concerning assumptions about the rate of these, and some other reactions involving only $A \leq 4$ elements. Furthermore, when regarding Fig. 7 in more detail, one also notes late-time production of ${}^6\text{Li}$ and ${}^7\text{Be}$ at some level due to the ${}^4\text{He}({}^2\text{H}-X^-, X^-){}^6\text{Li}$ as well as the ${}^6\text{Li}({}^1\text{H}-X^-, X^-){}^7\text{Be}$ reactions.

It is thus premature to conclude, that extreme ${}^6\text{Li}$ overproduction, rules out the existence of CHAMPs with long life times [23, 43]. The model shown above, at CHAMP densities many (five !) orders above those already claimed to be ruled out by ${}^6\text{Li}$ overproduction is observationally viable in all abundances. Constraints on the existence of CHAMPs in the early Universe could therefore, in principle, be much milder for long X^- life times than initially predicted. Nevertheless, they is further important physics entering the calculations discussed in the next two sections.

TABLE III: Assumed enhancement factor of a number of nuclear reactions between $A \leq 4$ nuclei involving bound states of $Z = 1$ nuclei. The Coulomb suppression factor is assumed to be completely absent in these reactions.

No.	$(AX) + B \rightarrow C + X$	enhancement
10	${}^2\text{H}({}^1\text{H}-X^-, X^-){}^3\text{He}$ ${}^1\text{H}({}^2\text{H}-X^-, X^-){}^3\text{He}$	1.25×10^2
11	${}^3\text{H}({}^1\text{H}-X^-, X^-){}^4\text{He}$ ${}^1\text{H}({}^3\text{H}-X^-, X^-){}^4\text{He}$	10.7
12	${}^2\text{H}({}^3\text{H}-X^-, n){}^4\text{He}+X^-$ ${}^3\text{H}({}^2\text{H}-X^-, n){}^4\text{He}+X^-$	1
13	${}^3\text{He}({}^2\text{H}-X^-, p){}^4\text{He}+X^-$	1

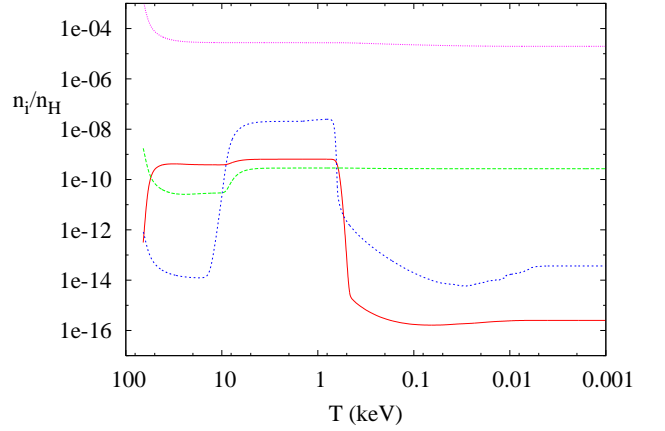


FIG. 7: Evolution of light-element number ratios ${}^7\text{Be}/{}^1\text{H}$ (solid - red), ${}^7\text{Li}/{}^1\text{H}$ (long-dashed - green), ${}^6\text{Li}/{}^1\text{H}$ (short-dashed - blue), and ${}^2\text{H}/{}^1\text{H}$ (dotted - purple), for a CHAMP model with $M_X = 100\text{ GeV}$, $\Omega_X h^2 = 0.01$, and $\tau_X = 10^{10}\text{ s}$. It is seen that large amounts of ${}^6\text{Li}$ and ${}^7\text{Be}$ synthesized at $T \approx 10\text{ keV}$ will be again destroyed at $T \approx 1\text{ keV}$. Neither effects due to electromagnetic and hadronic energy release during CHAMP decay nor charge exchange effects have been taken into account.

V. PHOTODISINTEGRATION OF BOUND STATES BY THE DECAY OF THE CHAMPS

There is another effect, heretofore overlooked, which may significantly reduce the in catalytic BBN at $T \approx 10\text{ keV}$ synthesized ${}^6\text{Li}$ (and ${}^7\text{Li}$) abundance. CHAMP decays are typically accompanied by the injection of electromagnetically interacting particles, with total energy comprising often a large fraction of the X rest mass. It is well-known, that such particles (e^- , e^+ , and γ 's) induce a rapid cascade on the cosmic blackbody photons, due to $\gamma\gamma_{\text{BB}}$ pair creation and inverse Compton scattering $e^\pm + \gamma$ processes, until the energy of any remaining γ 's is too low to further pair-produce, i.e. for $E_\gamma \lesssim E_{th} \approx m_e^2/22T \approx 1.2\text{ MeV}(T/10\text{ keV})^{-1}$. It is

seen, that this energy is above the binding energy of ${}^4\text{He}-X^-$ (and ${}^1\text{H}-X^-$) even at temperatures as high as $T \approx 30$ keV, making possible the ${}^4\text{He}-X^-$ and (${}^1\text{H}-X^-$) bound state photodisintegration before any significant ${}^6\text{Li}$ synthesis (destruction) has occurred. In Fig 8 the resultant photon spectrum due to the injection of energetic electromagnetically interacting particles at cosmic epochs with temperature $T = 10, 1$, and 0.1 keV is shown. The shown spectrum $E_\gamma dn_\gamma/d\ln E_\gamma$ is generated by a Monte-Carlo simulation taking account, not only of e^\pm pair production and inverse Compton scattering, but also $\gamma\gamma$ scattering (important at high $E_\gamma \lesssim E_{th}$, Bethe-Heitler pair production $\gamma + p, {}^4\text{He} \rightarrow p, {}^4\text{He} + e^- + e^+$, Compton scattering of the produced e^\pm , as well as the important Thomson (Klein-Nishina) scattering of γ 's on thermal electrons. It is based on the calculations presented in Ref. [37], with the Thomson scattering process extended to energies as low as $E_\gamma \approx 25$ keV, to account for ${}^1\text{H}-X^-$ destruction.

Following secondary and tertiary, etc. generations of scattered photons to obtain the correct photon spectrum for the bound state destructions process is mandatory. For example, the injection of 1 TeV of electromagnetically interacting energy at $T = 1$ keV is associated with injection of $N_\gamma \approx 3.3 \times 10^6$ primary photons with energy $E_\gamma \gtrsim 25$ keV, resulting from the initial cascade on the blackbody. When further interactions of these γ 's are considered the number rises to $N_\gamma \approx 1.1 \times 10^8$. In other words, an injected photon takes about 30 interactions before dropping below the threshold for ${}^1\text{H}-X^-$ photodisintegration. This exemplifies the importance of subsequent γ interactions. In Fig. 8 one may note a "pile-up" of photons at low E_γ . This is due to the typical fractional loss of γ 's in the Thomson regime $E_\gamma \lesssim m_e$ being small, such that it takes several Thomson scatterings for a photon to have dropped below $E_\gamma \lesssim E_{iH}^b \approx 25$ keV. A similar pile-up does not exist at $E_\gamma \lesssim E_{4He}^b \approx 350$ keV since during scatterings of γ 's with energy $E_\gamma \sim m_e$ on electrons the γ 's may lose a significant fraction of their energy. We thus expect the effects of photodisintegration of bound states have a larger impact on the ${}^1\text{H}-X^-$ bound state fraction than on that of ${}^4\text{He}-X^-$. This effect is not only due to the above, but also due to the photodisintegration cross section of ${}^1\text{H}-X^-$, $\sigma_{iH-X^-}^\gamma$ being larger than the one for ${}^4\text{He}-X^-$. Note that all calculations below, include numerically evaluated cross sections for the photodisintegration of all $A \leq 7$ nuclei bound states.

In Fig. 9 the bound state fractions in two scenarios: (a) of ${}^4\text{He}$ for a model with $\Omega_X h^2 = 0.1$ and $\tau_X = 3 \times 10^4$ s (and electromagnetic decay), and (b) of ${}^1\text{H}$ for $\Omega_X h^2 = 5 \times 10^{-3}$ and $\tau_X = 3 \times 10^6$ s, are shown in the same graph. Here the solid lines show f_{4He}^b (f_{iH}^b) when non-thermal bound state photodestruction is included, whereas the dotted lines show results when it is neglected. It is seen that realistic bound state fractions are significantly lower. In scenario (a) a ${}^6\text{Li}/\text{H}$ ratio ~ 10 times lower results, compared to when photodestruction is neglected, whereas in scenario (b) the ${}^6\text{Li}/\text{H}$ ratio is

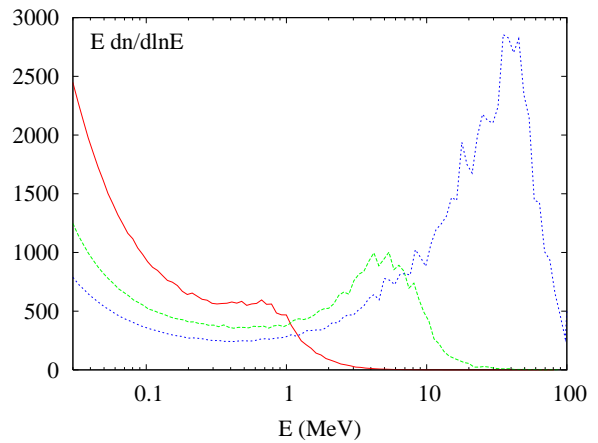


FIG. 8: Resultant photon spectrum $E_\gamma dn_\gamma/d\ln E_\gamma$ due to electromagnetic energy injection at cosmic epochs with temperatures at $T = 10$ keV (solid - red), 1 keV (dashed - green), and 0.1 keV (dotted - blue), respectively. The normalisation of the spectrum is arbitrary. The fraction of photons with energy above the ${}^4\text{He}-X^-$ photodisintegration threshold $E_4^b \approx 350$ keV is $\approx 1.9\%$, 3.7% , and 4.7% for temperatures $T = 10, 1$, and 0.1 keV, respectively.

~ 100 times higher. Here case (b) is affected by a reduced efficiency of ${}^6\text{Li}({}^1\text{H}-X^-, X^-){}^4\text{He} + {}^3\text{He}$, whereas in case (a) the reaction ${}^2\text{H}({}^4\text{He}-X^-, X^-){}^6\text{Li}$ is rendered less dominant. For sufficiently high Ω_X , and when thermal photodisintegration is unimportant, the resultant bound state fraction may be estimated by a steady state between the recombination rate, i.e. $\langle\sigma v\rangle_{\text{rec}} n_{4\text{He}} n_{X^-}$ and the photodisintegration rate, i.e. $\langle\sigma c\rangle_{\text{ph}} n_{({}^4\text{He}-X^-)} n_\gamma$. Here $n_{4\text{He}}$, $n_{({}^4\text{He}-X^-)}$, n_{X^-} , and n_γ are free ${}^4\text{He}$, bound ${}^4\text{He}$, X^- , and nonthermal photon number densities, respectively. The nonthermal photon number density n_γ may be obtained from $n_\gamma \approx dn_X/dt \tau_{Th} N_{E_b}^\gamma$ where $dn_X/dt \approx n_X/\tau_X$ before substantial decay, τ_{Th} is the life time of photons against Thomson scattering (i.e. the typical survival time), and $N_{E_b}^\gamma$ is the typical number of photons per particle decay with energy above the photodisintegration threshold E_b (including secondary generations). This, for example at $T = 1$ keV, is approximately 4×10^6 and 1×10^8 for ${}^4\text{He}$ and ${}^1\text{H}$ bound state photodisintegration, respectively, per 1 TeV of electromagnetically interacting energy injected into the plasma. It is thus found

$$f_{4He}^b \approx \frac{n_{({}^4\text{He}-X^-)}}{n_{4\text{He}}} \approx \frac{\langle\sigma v\rangle_{\text{rec}} \tau_X}{\langle\sigma c\rangle_{\text{ph}} \tau_{Th}} \frac{1}{N_{E_b}^\gamma} \quad (1)$$

It may be noted that this expression, which is valid only for large $Y_X \gtrsim 10^{-2}$ is independent of the CHAMP-to-baryon ratio, but dependent on the CHAMP life time.

VI. CHAMP EXCHANGE REACTIONS

It has been shown in Section 4 that the existence of only small fractions $f_p^b \sim 10^{-5}$ of protons in bound states,

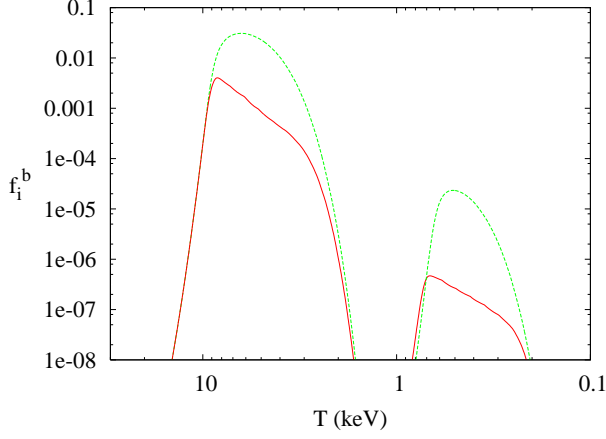


FIG. 9: ${}^4\text{He}$ bound state fraction f_4^b for a CHAMP BBN model (A) with $\Omega_X h^2 = 0.1$, $\tau_X = 3 \times 10^4 \text{s}$, and $f_{EM} = 1$ (the two curves on the left), and ${}^1\text{H}$ bound state fraction f_1^b for a CHAMP BBN model (B) with $\Omega_X h^2 = 5 \times 10^{-3}$, $\tau_X = 3 \times 10^6 \text{s}$, and $f_{EM} = 1$ (the two curves on the right). Solid (red) curves show f_i^b when photodisintegration of bound states due to electromagnetic energy release during the X -decay is included, whereas dashed (green) curves show results when this process is neglected. The resultant ${}^6\text{Li}$ yield in model (A) is ~ 10 times lower than when photodisintegration is excluded. Similarly, the resultant ${}^6\text{Li}$ yield in model (B) is ~ 100 times larger than without photodisintegration. CHAMP-exchange reactions have not been taken into account.

TABLE IV: Rates for CHAMP-exchange reactions computed in the Born approximation.

No.	$(AX) + B \rightarrow C + X$	rate [$\text{cm}^3 \text{s}^{-1}$]
14	$({}^1\text{H}-X^-) + {}^2\text{H} \rightarrow ({}^2\text{H}-X^-) + {}^1\text{H}$	8.8×10^{-15}
15	$({}^1\text{H}-X^-) + {}^3\text{H} \rightarrow ({}^3\text{H}-X^-) + {}^1\text{H}$	1.4×10^{-15}
16	$({}^2\text{H}-X^-) + {}^3\text{H} \rightarrow ({}^3\text{H}-X^-) + {}^2\text{H}$	1.0×10^{-14}
17	$({}^1\text{H}-X^-) + {}^4\text{He} \rightarrow ({}^4\text{He}-X^-) + {}^1\text{H}$	3.6×10^{-17}
18	$({}^2\text{H}-X^-) + {}^4\text{He} \rightarrow ({}^4\text{He}-X^-) + {}^2\text{H}$	2.9×10^{-16}
19	$({}^3\text{H}-X^-) + {}^4\text{He} \rightarrow ({}^4\text{He}-X^-) + {}^3\text{H}$	8.0×10^{-16}

forming below $T < 1 \text{keV}$, may efficiently destroy again any priorly synthesized ${}^6\text{Li}$ and ${}^7\text{Be}$. In Section 5 it has been seen that the efficiency of this destruction may be significantly reduced when non-thermal photodestruction of bound states is taken into account. In this section, a further important process reducing late-time ${}^6\text{Li}$ and ${}^9\text{Be}$ destruction is discussed. CHAMPs in bound states may exothermically transfer to heavier nuclei of equal or higher charge. In particular, $({}^1\text{H}-X^-)$ bound states could be removed by the $({}^1\text{H}-X^-) + {}^4\text{He} \rightarrow ({}^4\text{He}-X^-) + {}^1\text{H}$ charge exchange process. Charge exchange reactions turn out to be very important. In Table 4 the most important of these processes are presented. Rates for these processes were calculated in a very similar way, i.e.

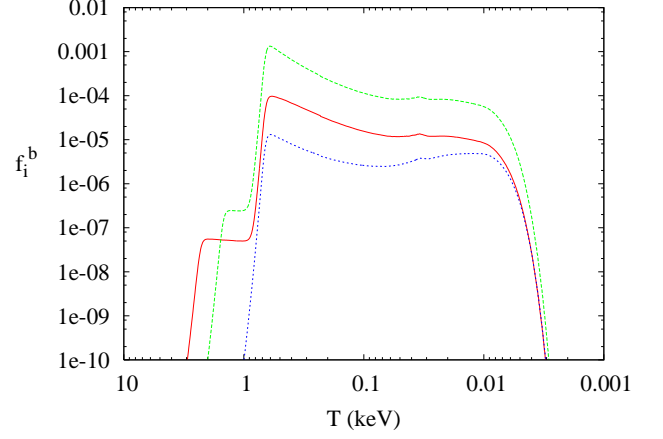


FIG. 10: As Fig. 5 but with charge exchange reactions included.

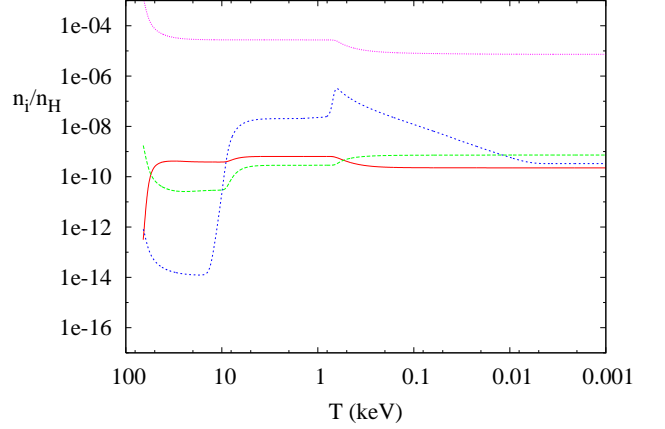


FIG. 11: As Fig. 7 but with charge exchange reactions included.

in the Born approximation, to those of nuclear reactions involving bound states, as presented in Appendix A. Here the dipole (quadrupole) operators Eq. (A4) (Eq. A5) replaced by the electromagnetic potential between the bound state and the heavier nucleus. The same arguments as presented in Section 3 apply concerning the failure of the Born approximation. In particular, rates given in Table 4 should be only considered as benchmarks, with the true rates possibly deviating significantly.

Fig. 10 shows bound state fractions for the same model as that shown in Fig. 5, but now with CHAMP exchange reactions included (photodisintegration of bound states is neglected). From the comparison of these two figures it is evident that whereas bound state fractions of ${}^1\text{H}$ in the absence of exchange reactions reach levels close to $f_p^b \approx 10^{-3}$, they are two orders of magnitude below when exchange reactions are present. This is mostly due to the $({}^1\text{H}-X^-) + {}^4\text{He} \rightarrow ({}^4\text{He}-X^-) + {}^1\text{H}$ reaction. A for the final BBN yield almost equally important change is the elevated ${}^2\text{H}$ (and ${}^3\text{H}$) bound state fraction when

the reactions in Table 4 are included. Though most ^1H exchange their CHAMPs with ^4He , due to the large ^4He abundance, a large fraction ~ 1 of ^2H enter bound states by capture of CHAMPs from protons as well. The ^2H bound state fraction in Fig. 10 (as well as Fig. 11) is only small $f_D^b \ll 1$, simply because once a ^2H (and ^3H) bound state has formed, its life time against destruction by reactions shown in Table 3, is very short. In other words, essentially each ^2H which enters a bound state will be subsequently destroyed, leading to the production of ^3He and ^4He . This will have important consequences for bounds on CHAMPs at larger CHAMP density, since either the lower bound on ^2H or the upper bound on $^3\text{He}/^2\text{H}$ may be violated. Fig. 11 shows the abundance evolution corresponding to Fig. 10, and is the equivalent to Fig. 7 but now with exchange reactions switched on. Several trends are visible: With charge exchange reactions the $^2\text{H}/\text{H}$ ratio has fallen below the observational lower limit, i.e. 7.4×10^{-6} compared to 2×10^{-5} in Fig. 7, the final $^7\text{Li}/\text{H}$ ratio is larger, i.e. 9.5×10^{-10} compared to 2.7×10^{-10} , and the $^6\text{Li}/\text{H}$ ratio is much larger, i.e. 3.3×10^{-10} compared to $\sim 4 \times 10^{-14}$. Here ^7Li is larger due to reduced $^7\text{Be}(^1\text{H}-X^-, X^-)^8\text{B}$ and enhanced $^4\text{He}(^3\text{H}-X^-, X^-)^7\text{Li}$ efficiencies, and ^6Li is larger due to reduced $^6\text{Li}(^1\text{H}-X^-, X^-)^4\text{He} + ^3\text{He}$ and enhanced $^4\text{He}(^2\text{H}-X^-, X^-)^6\text{Li}$ reactions.

When doing bound-state BBN computations with reactions on $Z = 1$ bound states as well as CHAMP exchange reactions included often very counter-intuitive results are obtained. As only one example, when the $(^1\text{H}-X^-) + ^2\text{H}$ rate is increased the ^6Li (and ^7Be) abundance may be reduced drastically. This is not what is expected since a lower $(^1\text{H}-X^-)$ and higher $(^2\text{H}-X^-)$ fraction ought to lead to a higher ^6Li abundance via enhanced $^4\text{He}(^2\text{H}-X^-, X^-)^6\text{Li}$ and reduced $^6\text{Li}(^1\text{H}-X^-, X^-)^4\text{He} + ^3\text{He}$. Nevertheless, this is not what happens, due to a higher $(^2\text{H}-X^-)$ fraction more ^2H is destroyed initially, rendering the $^4\text{He}(^2\text{H}-X^-, X^-)^6\text{Li}$ less effective at late times. Since the final abundance yield is given by the balance of the still fast processes of $^4\text{He}(^2\text{H}-X^-, X^-)^6\text{Li}$ production and $^6\text{Li}(^1\text{H}-X^-, X^-)^4\text{He} + ^3\text{He}$ destruction at late times less ^6Li results. Due to a lower $^6\text{Li}(^1\text{H}-X^-, X^-)^7\text{Be}$ efficiency less ^7Be results. Late-time bound-state BBN is very non-linear requiring full numerical integration up to late times to obtain reliable predictions.

VII. SOLUTIONS TO THE ^6Li AND ^7Li PROBLEMS DUE TO BOUND-STATE BBN FOR LONG-LIVED $\tau_x \gtrsim 10^6 \text{ SEC}$ CHAMPS ?

In Section 2 priorly proposed solutions to the ^7Li overabundance and ^6Li underabundance resulting within BBN in the presence of (relatively) short-lived CHAMPs have been discussed. Notwithstanding possible astrophysical explanations of these deviations between theory and observation, it has been shown that both problems

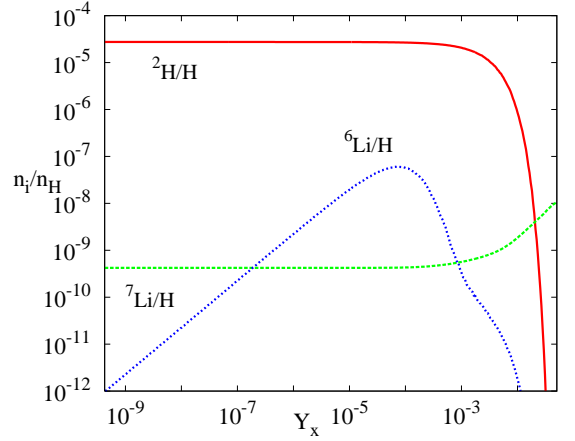


FIG. 12: Abundance yields of $^2\text{H}/\text{H}$ solid (red) $^7\text{Li}/\text{H}$ dashed (green), and $^6\text{Li}/\text{H}$ dotted (blue) as a function of CHAMP-to-baryon ratio Y_x for a model with $\tau_x = 10^{12} \text{ sec}$ and excluding electromagnetic- and hadronic- energy injection.

TABLE V: Three realizations of models which fulfill constraints on light-element abundances and reconcile predicted with observed $^7\text{Li}/^1\text{H}$ and $^6\text{Li}/^1\text{H}$ ratios. Shown are the CHAMP-to-baryon ratio as well as a list of reaction numbers and the respective factors by which these reactions rates have been multiplied with respect to the (unreliable) estimates in the Born approximation. All models have $\tau_x = 10^{12} \text{ s}$ and electromagnetic or hadronic energy injection has not been taken into account, corresponding to an invisible or almost mass-degenerate decay. Abundance yields in these models are shown in Table VI.

Model	Y_x	Reactions modified
A	4.3×10^{-4}	#4: 0.1 #7: 2. #14: 0.1 #17: 0.3
B	4.3×10^{-4}	#4: 0.3 #9: 0.3 #17: 0.1 #18: 30.
C	4.3×10^{-6}	#5: 3. #7: 30. #14: 0.03 #17: 0.03

may be solved at once in the presence of a decaying particle with decay time $\tau_x \approx 1000 \text{ s}$. This is possible in either case, a charged relic or a neutral relic. In subsequent sections it has been seen that late-time nucleosynthesis in the presence of charged weak-scale mass particles may lead to orders-of-magnitude modifications of the ^6Li , ^7Li , (and ^2H) abundances. It would be interesting to know

TABLE VI: The corresponding abundance yields resulting in the models shown in Table V.

Model	$^2\text{H}/\text{H}$	$^7\text{Li}/\text{H}$	$^6\text{Li}/\text{H}$
A	2.6×10^{-5}	2.8×10^{-10}	9.3×10^{-12}
B	2.4×10^{-5}	2.3×10^{-10}	3.7×10^{-11}
C	2.7×10^{-5}	1.5×10^{-10}	3.2×10^{-11}

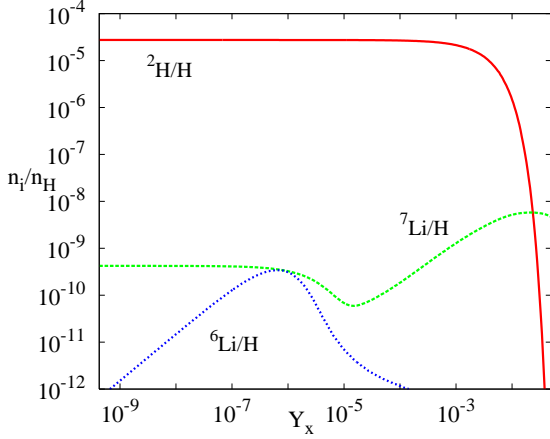


FIG. 13: As Fig. 13 but for reaction rates as in Model C shown in Table VI.

if CHAMPs with long life times $\tau_x \gtrsim 10^6$ s may reconcile the ${}^6\text{Li}$ and ${}^7\text{Li}$ discrepancies.

In Fig. 12 abundance yields for $\tau_x = 10^{12}$ s and varying Y_x are shown. Here reaction rates in the Born approximation were adopted and electromagnetic- and hadronic- energy injection due to the X decay was neglected, corresponding to, for example, an invisible decay or a decay to a neutral daughter particle almost degenerate in mass with the CHAMP. The model also approximates well the case of no decay, i.e. a stable CHAMP. At low CHAMP-to-baryon ratio Y_x only ${}^6\text{Li}$ is modified. Here most of the ${}^6\text{Li}$ is synthesized not at early times due to ${}^2\text{H}({}^4\text{He}-X^-, X^-){}^6\text{Li}$ but rather at late times due to ${}^4\text{He}({}^2\text{H}-X^-, X^-){}^6\text{Li}$. A small CHAMP density may therefore easily account for ${}^6\text{Li}$ in Pop II stars. When Y_x increases to 10^{-8} too much ${}^6\text{Li}$ is synthesized. For larger $Y_x \gtrsim 10^{-3}$ ${}^6\text{Li}$ destruction due to a high (${}^1\text{H}-X^-$) fraction reduces ${}^6\text{Li}$ again to observationally friendly levels. However, such models are then ruled out by ${}^7\text{Li}$ overproduction and ${}^2\text{H}$ underproduction, due to high (${}^2\text{H}-X^-$) and (${}^3\text{H}-X^-$) fractions, with ${}^7\text{Li}$ produced by ${}^3\text{H}({}^4\text{He}-X^-, X^-){}^7\text{Li}$ and ${}^2\text{H}$ destroyed by reactions given in Table 3. When the decay is electromagnetic or hadronic, with a large fraction $f_{EM} \sim 1$ of rest mass of X converted to electromagnetically interacting particles such high Y_x should in any case be ruled out due to elevated ${}^3\text{He}/{}^2\text{H}$ -ratios (cf. Ref. [37]).

Nevertheless, significant uncertainties exist due to the uncertainties in the bound-state nuclear reactions and charge exchange reactions. In Tables V and VI three (somewhat randomly chosen) models which do solve the ${}^6\text{Li}$ and ${}^7\text{Li}$ problems are shown. Here a number of reaction rates were scaled up (or down) from the Born approximation in order to arrive at an observationally satisfying result. It is seen that even at low Y_x such models may exist, depending on the exact magnitude of rates for a variety of reactions. It is also seen that, when going to lower Y_x , rates have to deviate more drastically from the Born approximation in order to solve the ${}^6\text{Li}$

TABLE VII: Adopted values for f_i^{cut} for the different reactions varied in the Monte-Carlo analysis (see text for details).

Reac. i	f_i^{cut}	Reac. i	f_i^{cut}
1	3	11	30
2	30	12	10
3	30	13	10
4	30	14	100
5	30	15	100
6	30	16	100
7	30	17	100
8	30	18	100
9	30	19	100
10	30		

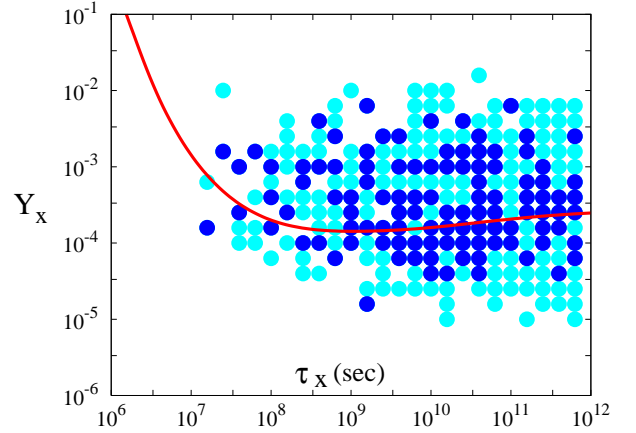


FIG. 14: Probability in the CHAMP-to-baryon Y_x - CHAMP life time τ_x parameter space at large τ_x that simultaneous solutions to the ${}^7\text{Li}$ and ${}^6\text{Li}$ (dark-blue) or only ${}^7\text{Li}$ (light-blue) problems exist. The points indicate 1 – 5% probability, whereas white areas had less than 1% of all randomly chosen reaction rates in the Monte-Carlo analysis result in ${}^6\text{Li}$ and ${}^7\text{Li}$ (or ${}^7\text{Li}$ only) solutions. No electromagnetic- or hadronic-energy release has been taken into account. Areas above the red line would be ruled out due to electromagnetic cascade nucleosynthesis under the assumption that $f_{EM} = 3 \times 10^{-2}$ of the rest mass of the CHAMP is converted to electromagnetically interacting energy. See text for further detail.

and ${}^7\text{Li}$ problems. The corresponding abundance yields for Model C, where at low Y_x observationally satisfying results are obtained, are shown in Fig. 13. The figure clearly indicates that parameter space for a reduction of ${}^7\text{Li}$ and production of some ${}^6\text{Li}$ exists.

In the absence of reliable estimates for reaction rates it is difficult to assess quantitatively if significant parameter space for simultaneous solutions for the ${}^6\text{Li}$ and ${}^7\text{Li}$ discrepancies for late decaying $\tau_X \gtrsim 10^6$ sec CHAMPs exist. In particular all nuclear reactions shown in Table II and Table III, as well as the charge exchange reactions

shown in Table IV, i.e. a total number of nineteen reactions. Though all rates have been determined numerically in the Born approximation in this paper, as the Born approximation is likely to fail badly, results become uncertain. In order to still arrive at a reliable result one is thus forced to perform a Monte-Carlo analysis, varying all ill-determined reaction rates within conservative ranges. This has been done in the present paper. In particular, the Born approximation values of the rates shown in Figs. 3 and 4, as well as given in Table III and IV, have been taken as benchmarks. For each reaction a random generator determined a factor f_i with which the benchmark rate was multiplied. These factors were generated with a probability distribution flat in logarithmic space, and between values $1/f_i^{cut} \leq f_i \leq f_i^{cut}$. For the reaction-rate dependent conservatively chosen f_i^{cut} the reader is referred to Table VII. For each point in parameter space, i.e. for Y_x and τ_x , this procedure was repeated a 1000 times in order to arrive with one thousand different randomly chosen sets for the 19 ill-determined reaction rates. For each realization of reaction rates an independent BBN calculation was then performed and compared to the observational constraints.

The results of this Monte-Carlo analysis are shown in Fig. 14. Here dark (dark-blue) area indicates the probability that between 1% - 5% (i.e. 10-50) of all independent 1000 BBN calculations with randomly varied rates respect the abundance limits on other light elements (as given in Ref. [37]) while fulfilling ${}^7\text{Li}/{}^1\text{H} < 2.5 \times 10^{-10}$ and $0.66 > {}^6\text{Li}/{}^7\text{Li} > 0.03$. Similarly, light (light-blue) areas indicate the same, but with now only the ${}^7\text{Li}$ discrepancy solved (i.e. ${}^6\text{Li}/{}^7\text{Li} < 0.03$) is acceptable). It is noted that in none of the parameter space a probability $> 5\%$ for ${}^6\text{Li} + {}^7\text{Li}$ (or only ${}^7\text{Li}$) solving areas is found, indicating that the reaction rate combinations which may yield such solutions are rather rare. The likelihood for such scenarios is even further diminished when electromagnetic- and/or hadronic- energy injection due to the decay of the particle is considered. In fact, when $f_{EM} \sim 1$ all of the parameter space shown in Fig. 14 capable of solving the ${}^6\text{Li} + {}^7\text{Li}$ problems simultaneously (though at a $< 5\%$ likelihood), would be completely eliminated. Only when f_{EM} is rather small, some area remains. This is shown by the (red) line for $f_{EM} = 3 \times 10^{-2}$ corresponding, for example, to the decay of a stau $\tilde{\tau}$ to a tau and gravitino, with the gravitino only 10% lighter than the stau. The area above the line is ruled out by overproduction of the ${}^3\text{He}/{}^2\text{H}$ ratio due to ${}^4\text{He}$ photodisintegration. On the other hand, not shown in Fig. 14 are areas where only the ${}^6\text{Li}$ abundance as observed in Pop II stars may be produced. These exist plentiful, and at high probability, in particular at lower $Y_x \lesssim 10^{-5}$. It thus seems unlikely that CHAMPs with $\tau_x \gtrsim 10^6\text{sec}$ may resolve the ${}^7\text{Li}$ problem, though they could possibly constitute the source for the observed ${}^6\text{Li}$ at low metallicity.

VIII. CONCLUSIONS

In summary, I have presented results of a very detailed study of BBN in the presence of negatively charged massive particles (CHAMPs). Such particles have been shown to form bound states with nuclei towards the end of a conventional BBN epoch [23, 24, 25, 26, 27, 28, 29] and may alter BBN yields due to the catalysis of nuclear reactions [23]. The present analysis attempts to take into account of all relevant effects for making relatively precise predictions of catalytic light-element nucleosynthesis for nuclei with $A \leq 7$, but excluding the formation of molecules. It includes numerical evaluations in the Born approximation of all key nuclear cross sections, where one of the nuclei is in a bound state. Bound-state recombination and photodisintegration cross sections are also determined numerically. Furthermore, three very important and priorly not treated effects for the CHAMP BBN at late times $\tau \gtrsim 10^5\text{sec}$ are included: (a) rapid nuclear reactions including charge $Z = 1$ nuclei in bound states, (b) the photodisintegration of bound states due to γ - and x - rays generated during the decay of the CHAMPs, and (c) CHAMP-exchange reactions from a bound state within a lighter nucleus to a bound state within a heavier nucleus. Light element abundances and bound state fractions are computed without approximations. The effects of hadronic and electromagnetic cascades due to CHAMP disintegration on light element abundances are properly taken into account.

The present detailed study reveals that bound-state BBN proceeds very differently than initially forecasted [23, 24]. At low temperatures $T \lesssim 1\text{keV}$, a large number ~ 20 of Coulomb-barrier unsuppressed nuclear reactions and charge exchange reactions become operative and are capable, in most of the parameter space, to change ${}^6\text{Li}$, ${}^7\text{Li}$, and ${}^2\text{H}$ abundances by orders of magnitude. Unfortunately, reaction rates for these processes are not well approximated by the Born approximation, such that for CHAMP life times $\tau_x \gtrsim 10^5\text{sec}$ one has to resort to a Monte-Carlo analysis.

The purpose of this study is to investigate the potential of CHAMP BBN to resolve the current ${}^6\text{Li}$ and ${}^7\text{Li}$ discrepancies between standard BBN and observations. It is shown, that a priorly proposed simultaneous solution of the ${}^6\text{Li}$ and ${}^7\text{Li}$ problems with a relic particle decaying at $\tau_x \approx 1000\text{sec}$ [21], is not very dependent on the decaying relic being charged [35] or not, unless its hadronic branching ratio is well below $B_h \lesssim 10^{-4}$. A solution with $B_h \ll 10^{-4}$ has, however, the advantage to not change much the ${}^2\text{H}/{}^1\text{H}$ ratio from its respective standard BBN value. Since ${}^6\text{Li}$ and ${}^7\text{Li}$ may be rapidly destroyed at late times one generically expects further simultaneous solutions of the ${}^6\text{Li}$ and ${}^7\text{Li}$ problems for $\tau_x \gtrsim 10^6\text{sec}$. Nevertheless, even given the current reaction rate uncertainties, a Monte-Carlo shows that only a very small fraction $\lesssim 5\%$ of reaction rate combinations may lead to such solutions. Since such possible solutions occur at relatively high CHAMP-to-baryon ratio $3 \times 10^{-5} \lesssim Y_x \lesssim 10^{-2}$ they

are further constrained by the effects of electromagnetic energy injection and possible ${}^3\text{He}/{}^2\text{H}$ overproduction, requiring the decay to be invisible, or mother and daughter particle to be somewhat degenerate in mass $\sim 10\%$. On the other hand, CHAMPs may well be the source of the observed ${}^6\text{Li}$ at low metallicity.

I acknowledge helpful discussions with and M. Asplund, S. Bailly, O. Kartavtsev, K. Kohri, A. Korn, G. Moulaka, M. Pospelov, J. Rafelski, G. Starkman, V. Tatischeff, and T. Yanagida.

APPENDIX A: THERMONUCLEAR REACTIONS IN THE PRESENCE OF BOUND STATES IN THE BORN APPROXIMATION

Consider the three-body system of nuclei A , B , and CHAMP X^- . Since for weak scale mass CHAMPs and light nuclei $M_X \gg M_A, M_B$, it is an excellent approximation to assume X^- to be at rest at the origin, effectively acting as an external potential which absorbs momentum but not energy. The Hamiltonian of the system is then given by

$$H = \frac{1}{2}M_A\dot{\mathbf{r}}_A^2 + \frac{1}{2}M_B\dot{\mathbf{r}}_B^2 + V_C(|\mathbf{r}_A - \mathbf{r}_B|) + V_{\text{NUC}}(\mathbf{r}_A, \mathbf{r}_B) - \frac{Z_A e^2}{r_A} - \frac{Z_B e^2}{r_B}, \quad (\text{A1})$$

where $\mathbf{r}_A, \mathbf{r}_B$ represent the position vectors of nuclei A and B , r_A, r_B their magnitudes, and $Z_A e, Z_B e$ their respective charges. In Eq. (A1) the first two terms represent kinetic energies, the second and third term, Coulomb and nuclear potentials between A and B , and the last terms, the Coulomb potentials between the (assumed singly charged) CHAMP X^- and the nuclei. This Hamiltonian will be split into a dominant contribution H_0 and a perturbative contribution $H_1 \ll H_0$. In a rearrangement reaction of the type $(A - X^-) + B \rightarrow C + X^-$, where C is a nuclear bound state between A and B , the unperturbed and perturbed Hamiltonians for initial and final states are different, i.e. $H_0^i \neq H_0^f, H_1^i \neq H_1^f$. In particular, whereas in the initial state the perturbation is best chosen as the nuclear attraction between A and B , i.e. $H_1^i = V_{\text{NUC}}$ and $H_0^i = H - H_1^i$, in the final state it will be the differential Coulomb force of X^- on the nuclear bound state $C = (A - B)$. When initial and final states are chosen as eigenstates to H_0^i and H_0^f , respectively, standard methods show that, in the Born approximation the transition amplitude may be computed by either $\langle i | H_1^f | f \rangle$ or $\langle f | H_0^i | i \rangle$. The initial and final states are chosen as

$$|i\rangle = |\Phi_{(A-X^-)}(\mathbf{r}_A)\rangle |\Phi_{\text{Coul}}(\mathbf{r}_B)\rangle \quad (\text{A2})$$

$$|f\rangle = |\Phi_{(A-B)}(\rho)\rangle |\Phi_{\text{Coul}}(\mathbf{s})\rangle \quad (\text{A3})$$

where \mathbf{s} and ρ are the $A - B$ center of mass and relative coordinates, respectively. Coulomb wave func-

tions $|\Phi_{\text{Coul}}\rangle$ and the $A - X^-$ bound state wave function $\Phi_{(A-X^-)}$ were determined numerically with realistic charge distributions. The nuclear wave function $\Phi_{(A-B)}$ was parametrised by $\Phi = 2\sqrt{\gamma^5/3}\rho \exp(-\gamma\rho)$ with γ adjusted such that in the absence of X^- the correct experimentally determined cross section results. The perturbation H_1^f was chosen as the first non-vanishing element in the expansion of the last two terms of Eq. (A1) in terms of relative coordinate ρ . For dipole transitions this results into

$$H_1^f = -(Z_A R_A + Z_B R_B) e^2 \frac{s_i \rho_i}{s^3} \quad (\text{A4})$$

whereas for quadrupole transitions

$$H_1^f = -(Z_A R_A^2 + Z_B R_B^2) e^2 \left(\frac{3}{2} \frac{s_i s_j \rho_i \rho_j}{s^5} - \frac{1}{2} \frac{\rho^2}{s^3} \right) \quad (\text{A5})$$

where $R_A = M_B/(M_A + M_B)$ and $R_B = -M_A/(M_A + M_B)$. Rates were evaluated by numerical integration of the matrix elements $\langle i | H_1^f | f \rangle$ employing Fermi's Golden rule

$$\sigma v = \frac{2\pi}{\hbar} V \int dN_f \delta(E_i - E_f) |\langle i | H_1^f | f \rangle|^2 \quad (\text{A6})$$

where V is a normalization volume, v relative velocity, δ the Delta-function, and

$$dN_f = \frac{V}{(2\pi\hbar)^3} p_C^2 dp_C d\Omega_C \quad (\text{A7})$$

a measure of the final phase space for nucleus C . For the evaluation of the matrix elements, six-dimensional integrals over the coordinates of two nuclei could be analytically reduced to three-dimensional integrals which were numerically evaluated. Similiar to Ref. [31] I have not considered internal spin of the nuclei, except for the obvious total angular momentum degeneracy factors. Finally cross sections $\sigma(E)$ were converted to S-factors $S(E)$. They are related by

$$\sigma(E) = (S(E)/E) \exp(-G(E)), \quad (\text{A8})$$

where E is center-of mass (CM) energy and $\exp(G)$ with

$$G(E) = \frac{2\pi(Z_A - 1)Z_B \alpha c}{v_{\text{CM}}} \quad (\text{A9})$$

is the Coulomb repulsion factor. In the above v_{CM} is the relative velocity ($v_{\text{CM}} \approx v_B$ for bound states), and α, c fine structure constant and speed of light, respectively. For assumptions concerning the angular momentum of the final $A-B$ nucleus, the number of multipoles included in the calculation, and the assumed S-factor in the absence of bound states the reader is referred to Table 2. The determined S-factors were subsequently integrated over a thermal distribution to derive thermal nuclear rates in the presence of bound states.

-
- [1] D. N. Spergel *et al.*, astro-ph/0603449.
- [2] F. Spite and M. Spite, *Astronomy & Astrophysics* **115**, 357 (1982); P. Bonifacio and P. Molaro, *MNRAS* **285**, 847 (1997); S. G. Ryan, T. C. Beers, K. A. Olive, B. D. Fields and J. E. Norris, *Astrophys. J. Lett.* **530**, L57 (2000); P. Bonifacio *et al.*, *Astronomy & Astrophysics* **390**, 91 (2002); J. Melendez and I. Ramirez, *Astrophys. J.* **615**, L33 (2004); C. Charbonnel and F. Primas, *Astronomy & Astrophysics* **442**, 961 (2005).
- [3] M. Asplund, D. L. Lambert, P. E. Nissen, F. Primas and V. V. Smith, *Astrophys. J.* **644**, 229 (2006).
- [4] for former ${}^6\text{Li}$ detections cf. to: V. V. Smith, D. L. Lambert, and P. E. Nissen, *Astrophys. J.* **408**, 262 (1993); **506**, 405 (1998); L. M. Hobbs and J. A. Thorburn, *Astrophys. J.* **491**, 772 (1997); R. Cayrel, M. Spite, F. Spite, E. Vangioni-Flam, M. Cassé, and J. Audouze, *Astron. & Astrophys.* **343**, 923 (1999); P. E. Nissen, M. Asplund, V. Hill, and S. D’Odorico, *Astr. & Astrophys.* **357**, L49 (2000).
- [5] calculations by Richard *et al.* [6] presented in Ref. [3].
- [6] O. Richard, G. Michaud, and J. Richer, *Astrophys. J.*, **580**, 1100 (2002); O. Richard, G. Michaud, and J. Richer, *Astrophys. J.*, **619**, 538 (2005).
- [7] M. Salaris and A. Weiss, *Astron. Astrophys.* **376**, 955 (2001); M. H. Pinsonneault, G. Steigman, T. P. Walker, K. Narayanan and V. K. Narayanan, *Astrophys. J.* **574**, 398 (2002); S. Talon and C. Charbonnel, *Astronomy & Astrophysics* **418**, 1051 (2004); A. M. Boesgaard, A. Stephens and C. P. Deliyannis, *Astrophys. J.* **633**, 398 (2005); L. Piau, arXiv:astro-ph/0511402.
- [8] A. J. Korn *et al.*, *Nature* **442**, 657 (2006).
- [9] F. Confortola *et al.* [LUNA Collaboration], *Phys. Rev. C* **75**, 065803 (2007).
- [10] cf., for example, to E. Vangioni-Flam, M. Casse and J. Audouze, *Phys. Rept.* **333**, 365 (2000); R. Ramaty, S. T. Scully, R. E. Lingenfelter and B. Kozlovsky, *Astrophys. J.* **534**, 747 (2000).
- [11] S. Inoue and T. K. Suzuki, *Nucl. Phys. A* **718**, 69 (2003).
- [12] N. Prantzos, arXiv:astro-ph/0510122.
- [13] B. B. Nath, P. Madau and J. Silk, *Mon. Not. Roy. Astron. Soc. Lett.* **366**, L35 (2006).
- [14] V. Tatischeff and J. P. Thibaud, arXiv:astro-ph/0610756.
- [15] K. Jedamzik, *Phys. Rev. Lett.* **84**, 3248 (2000).
- [16] For a recent re-analysis, cf. to M. Kusakabe, T. Kajino and G. J. Mathews, *Phys. Rev. D* **74**, 023526 (2006).
- [17] S. Dimopoulos, R. Esmailzadeh, L. J. Hall and G. D. Starkman, *Astrophys. J.* **330**, 545 (1988).
- [18] K. Jedamzik, *Phys. Rev. D* **70**, 083510 (2004).
- [19] J. L. Feng, A. Rajaraman and F. Takayama, *Phys. Rev. D* **68**, 063504 (2003).
- [20] J. R. Ellis, K. A. Olive and E. Vangioni, *Phys. Lett. B* **619**, 30 (2005).
- [21] K. Jedamzik, *Phys. Rev. D* **70**, 063524 (2004).
- [22] K. Jedamzik, K. Y. Choi, L. Roszkowski and R. Ruiz de Austri, *JCAP* **0607**, 007 (2006).
- [23] M. Pospelov, arXiv:hep-ph/0605215.
- [24] K. Kohri and F. Takayama, arXiv:hep-ph/0605243.
- [25] M. Kaplinghat and A. Rajaraman, *Phys. Rev. D* **74**, 103004 (2006).
- [26] D. Fargion, M. Khlopov and C. A. Stephan, *Class. Quant. Grav.* **23**, 7305 (2006).
- [27] A. De Rujula, S. L. Glashow and U. Sarid, *Nucl. Phys. B* **333**, 173 (1990).
- [28] S. Dimopoulos, D. Eichler, R. Esmailzadeh and G. D. Starkman, *Phys. Rev. D* **41**, 2388 (1990).
- [29] J. Rafelski, M. Sawicki, M. Gajda and D. Harley, *Phys. Rev. A* **44**, 4345 (1991).
- [30] R. H. Cyburt, J. R. Ellis, B. D. Fields, K. A. Olive and V. C. Spanos, *JCAP* **0611**, 014 (2006).
- [31] K. Hamaguchi, T. Hatsuda, M. Kamimura, Y. Kino and T. T. Yanagida, arXiv:hep-ph/0702274.
- [32] J. Pradler and F. D. Steffen, *Phys. Lett. B* **648**, 224 (2007).
- [33] Reaction rates, for example, for neutrons on ${}^7\text{Be}$, are given by the product of their reaction cross section σ and the relative velocity between the reacting nuclei, v . It is argued that due to the fast motion of the ${}^7\text{Be}$ nucleus around the CHAMP, the relative velocity v could be enhanced by orders of magnitude. This is clearly not so, as v is, simply, part of the flux factor at large distances, defining the flux of incoming neutrons in the cosmic rest frame, which is essentially the rest frame of the heavy ${}^7\text{Be}-X^-$ bound system. Due to the small thermal velocities of the heavy bound state, the relative velocity, and thus the reaction rate, is even reduced, but only about a factor of order unity. See also Ref. [35] for a more detailed discussion.
- [34] D. Cumberbatch, K. Ichikawa, M. Kawasaki, K. Kohri, J. Silk and G. D. Starkman, arXiv:0708.0095 [astro-ph].
- [35] C. Bird, K. Koopmans and M. Pospelov, arXiv:hep-ph/0703096.
- [36] T. Jittoh, K. Kohri, M. Koike, J. Sato, T. Shimomura and M. Yamanaka, arXiv:0704.2914 [hep-ph].
- [37] K. Jedamzik, *Phys. Rev. D* **74**, 103509 (2006).
- [38] The Bohr radius is only given for illustrative purposes, all calculations assume bound state wave functions determined by the Schroedinger equation, and deviating significantly from the $1s$ Bohr wave function. The approximative Bohr radius was determined by requiring the same asymptotic slope at larger distances.
- [39] For example, the rapid ${}^6\text{Li}(p, \alpha){}^3\text{He}$ rate for $T \gtrsim 10\text{ keV}$, continuously destroys ${}^6\text{Li}-X^-$ bound states, such that the ${}^6\text{Li}$ bound state fraction is below that expected from naive estimates.
- [40] A necessary requirement for the validity of the Born approximation is $H_p/E_i \ll 1$, where H_p is the perturbative Hamiltonian and E_i is the initial energy. I acknowledge private communication with T. Yanagida on this point.
- [41] Throughout the paper, it is assumed that only half of the stated Ω_X abundance is within negatively charged species X^- , with the other half in the antiparticle of X , i.e. X^+ , such that electrical neutrality is kept.
- [42] Naively thought, some of the ${}^7\text{Li}$ (synthesized as ${}^7\text{Be}$) could survive the rapid ${}^7\text{Be}({}^1\text{H}-X^-, X^-){}^8\text{B}$ destruction reaction at $T \approx 1\text{ keV}$ if ${}^7\text{Be}$ would be converted to ${}^7\text{Li}$ at $\tau \lesssim 10^6\text{ s}$. In fact, the half life for ${}^7\text{Be}$ against electron capture is $\tau_{\text{Be}} \approx 4.6 \times 10^6\text{ s}$. Nevertheless, the binding energy of an electron to the ${}^7\text{Be}$ nucleus is $E_b \approx 0.21\text{ keV}$, such that the ${}^7\text{Be}$ nucleus stays bare until much lower temperatures $T \ll 1\text{ keV}$. Since the electron plasma density is well below the effective density of electrons in a recombined ${}^7\text{Be}$ nucleus, the ${}^7\text{Be}$ nuclei has to either await

recombination or β^+ -decay to convert to ${}^7\text{Li}$. Due to the rapidness of the ${}^7\text{Be}$ destruction process, it is therefore expected that ${}^7\text{Be} \rightarrow {}^7\text{Li}$ at low temperatures plays hardly a role.

[43] M. Kawasaki, K. Kohri and T. Moroi, Phys. Lett. B **649**,

436 (2007)

[44] The effects of annihilation of X^- with X^+ in $X^- - X^+$ bound states forming to some degree [35] are subdominant compared to those of the decay itself.